Astronomy & Astrophysics manuscript no. 7613
February 1, 2008

Observing the gas temperature drop in the high-density nucleus of L 1544.⋆

Antonio Crapsi[1,2], Paola Caselli[1,3], Malcolm C. Walmsley[1], and Mario Tafalla[4]

[1] Osservatorio Astrofisico di Arcetri, Largo E. Fermi, 5, I-50125, Firenze, Italy
[2] Leiden Observatory, Leiden University, P.O. Box 9513, NL-2300 RA, Leiden, The Netherlands
[3] Harvard-Smithsonian Center for Astrophysics, 60 Garden St., MS 42, Cambridge, MA 02138, USA
[4] Observatorio Astronómico Nacional (IGN), Alfonso XII, 3, E-28014, Madrid, Spain

Received 05 April 2007 / Accepted 27 April 2007

ABSTRACT

Context. The thermal structure of a starless core is crucial for our understanding of the physics in these objects and hence for our understanding of star formation. Theory predicts a gas temperature drop in the inner ∼5000 AU of these objects, but there has been no observational proof of this.

Aims. We performed VLA observations of the NH_3 (1,1) and (2,2) transitions towards the pre-stellar core L 1544 in order to measure the temperature gradient between the high density core nucleus and the surrounding core envelope. Our VLA observation for the first time provide measurements of gas temperature in a core with a resolution smaller than 1000 AU. We have also obtained high resolution Plateau de Bure observations of the 110 GHz $1_{11} - 1_{01}$ para–NH_2D line in order to further constrain the physical parameters of the high density nucleus.

Methods. We combine our interferometric NH_3 and NH_2D observations with available single dish measurements in order to estimate the effects of flux loss from extended components upon our data. We have estimated the temperature gradient using a model of the source to fit our data in the *u*, *v* plane. As the NH_3(1,1) line is extremely optically thick, this also involved fitting a gradient in the NH_3 abundance. In this way, we also measure the [NH_2D]/[NH_3] abundance ratio in the inner nucleus.

Results. We find that indeed the temperature decreases toward the core nucleus from 12 K down to 5.5 K resulting in an increase of a factor of 50% in the estimated density of the core from the dust continuum if compared with the estimates done with constant temperature of 8.75 K. Current models of the thermal equilibrium can describe consistently the observed temperature and density in this object, simultaneously fitting our temperature profile and the continuum emission. We also found a remarkably high abundance of deuterated ammonia with respect to the ammonia abundance (50%±20%), which proves the persistence of nitrogen bearing molecules at very high densities ($2 \cdot 10^6$ cm^{-3}) and shows that high-resolution observations yield higher deuteration values than single-dish observations. The NH_2D observed transition, free of the optical depth problems that affect the NH_3 lines in the core center, are a much better probe of the high-density nucleus and, in fact, its map peak at the dust continuum peak. Our analysis of the NH_3 and NH_2D kinematic fields shows a decrease of specific angular momentum from the large scales to the small scales.

Key words. ISM: clouds – ISM: evolution – ISM: individual(L 1544) – ISM: molecules – Stars: formation – Techniques: interferometric

1. Introduction

Dense starless cores are thought to be the forerunners of solar mass protostars and hence determining their physical and chemical evolution is an essential step in our understanding of star formation. Thus, measuring their physical characteristics (temperature,density, velocity field) should give us insight into the initial conditions just prior to the collapse of a protostar. Most interesting in this regard are the cores of highest central density and column density which appear closest to the "pivotal structure" in which the core is on the verge of instability.

Recent observations of both the dust continuum and molecular lines have allowed a selection to be made of the cores of highest central density (Ward-Thompson et al. 1999; Tafalla et al. 2002; Crapsi et al. 2005). It turns out that such cores have a few other properties in common such as high deuterium fractionation and (in a few cases) some evidence for increased velocity dispersion indicative of contraction in the high density core nucleus. Deuterium fractionation potentially gives us important information on the ionization fraction at high densities while the observed velocities and line widths yield precious information on angular momentum and infall. To exploit these to the full however requires high angular resolution measurements in a nearby core. With this in mind, we decided to obtain high quality interferometer maps of the nearby Taurus core L 1544 in the 23 GHz (J,K)=(1,1) and (2,2) lines of ammonia (NH_3)as well as in the 110 GHz $1_{11} - 1_{01}$ transition of deuterated ammonia (para–NH_2D).

The choice of ammonia and NH_2D for this study was partly based on the fact that it has been found (e.g. Tafalla et al. 2004) that nitrogen containing species such as ammonia and its deuterium isotopologues trace preferentially the densest gas in nearby cores. The reason for this is not precisely known but is likely to be related to the relative volatility of both atomic and

Send offprint requests to: Antonio Crapsi, e-mail: crapsi@arcetri.astro.it

⋆ Based on observations carried out with the IRAM Plateau de Bure Interferometer and the Very Large Array. IRAM is supported by INSU/CNRS (France), MPG (Germany) and IGN (Spain). The National Radio Astronomy Observatory is a facility of the National Science Foundation operated under cooperative agreement by Associated Universities, Inc.

molecular nitrogen. It is also important that the relative population of the (1,1) and (2,2) levels of ammonia is an excellent temperature indicator (see e.g. Ho & Townes 1983; Danby et al. 1988; Ungerechts et al. 1986) due to the fact that radiative transitions between the K=2 and K=1 ladders of NH_3 are forbidden. We can therefore use the relative optical depths in these two lines as a measure of temperature. One of the basic questions about pre-stellar cores is whether they have a positive temperature gradient outwards (see e.g. Leung 1975; Evans et al. 2001; Zucconi et al. 2001; Galli et al. 2002; Lesaffre et al. 2005) with temperatures of the order of 6 K in their center, as one would expect from theoretical considerations. On large scales > 0.05 pc, there is already evidence for higher dust temperatures on core edges than in core centers (Ward-Thompson et al. 2002; Pagani et al. 2004; Kirk et al. 2005) but on the scale of 0.01 pc (15″ at 140 pc), the situation is less clear. With this in mind, we obtained and present in this work D-array VLA NH_3 observations with a roughly 4″synthesised beam . We are thus sensitive to compact structure of size roughly 1000 AU.

Measuring the temperature gradient is of importance mainly as a test of our understanding of the thermodynamics of pre-stellar cores though it also is of some importance for the core stability (see Galli et al. 2002). The temperature measurements test our understanding of dust–gas coupling and CO cooling (see e.g. Bergin et al. 2006). They are also important for the interpretation of dust continuum emission maps where it is usual to assume an isothermal dust temperature and spherical symmetry in order to derive the density distribution. The latter is often not valid as we discuss later (Gonçalves et al. 2004; Doty et al. 2005) but is nevertheless a useful zero order approximation. Detailed modelling of L 1544 has been carried out by Doty et al. (2005) who fit the mm–submm continuum data of that source with a dust temperature drop from 15 K to 5.4 K. We note however that the ammonia single dish data for several sources including L 1544 show no evidence for gradients (Tafalla et al. 2002, 2004) and thus the existence of temperature gradients in pre-stellar cores is uncertain.

L 1544 is a well-studied low-mass starless core in Taurus, which presents a large central density (> 10^6 cm^{-3}), considerable CO freeze-out (> 93%) and high degree of deuteration (N_2D^+/N_2H^+ ∼0.25). These properties, combined with kinematical probes of infall (differences in velocity between thin and thick tracers, and increasing line widths of thin tracers toward the core centre) makes this core a good candidate for being on the point of becoming unstable (Crapsi et al. 2005). One expects the dynamics of the inner core to be better sampled by deuterated species and we have therefore obtained high resolution observations of the $1_{11} - 1_{01}$ transition of para–NH_2Dat 110 GHz with the IRAM Plateau de Bure interferometer (PdBI). The resolution is rather similar to that of the VLA and we are thus able to measure the deuterium fractionation in the core nucleus. We also can derive important limits on angular momentum and infall.

This paper is organized as follows, in section 2 we report the details of the VLA and PdBI observing runs, in section 3 we present our basic results, in section 4 we describe our analysis procedure and in section 5 we summarize our results.

2. Observations

We used the Very Large Array (VLA) to observe L 1544 in the (1,1) and (2,2) transitions of para-NH_3 (at 23694.4949 MHz and 23722.6349 MHz respectively) and the Plateau de Bure interferometer (PdBI) to observe the $(1_{1,1} - 1_{0,1})$ transition of para–NH_2D (at 110153.587 MHz). The reference position we used in this work is the dust continuum peak taken from the 1.2 mm map of Ward-Thompson et al. (1999): (05:04:17.230, 25:10:47.70) J2000.0.

2.1. VLA Observations

Observations at the VLA were performed in compact configuration (D) on March 8th, 2003 and April 3rd, 2003 for a total of 20 hours of observations. On-source observations were interleaved by the quasar 0510+180 (1 Jy at 1.3 cm according to the VLA calibrator manual[1]) for phase calibration, whereas absolute flux calibration was performed using 3C286 (2.59 Jy at 1.3 cm). The difference in average flux density for 0510+180 between the two observing runs was ∼15% and we take this as the uncertainty in flux calibration. The NH_3(1,1) and (2,2) data were acquired simultaneously using the 2 IF spectral line mode, sampling 64 channels over two 781 kHz (or 9.8 km s^{-1}) bandwidths and reaching a channel width of 12.2 kHz (or 0.154 km s^{-1}). While the (2,2) band was centred at the main hyperfine rest frequency, the (1,1) band was offset by 306 kHz to include both the main group of hyperfines and one secondary group (F_1=2-1 at 23693.905 MHz) of hyperfines. The VLA primary beam at the ammonia frequencies is 2′, while the synthesized beam, after applying natural weighting, reached 4.″34×3.″45 with a position angle (PA) of 79.°9. In order to increase the signal-to-noise ratio we reconstructed the clean map of the NH_3(2,2) using a circular clean beam with full width at half power of 8″. Calibration and data reduction were performed using the Astronomical Image Processing System (AIPS) of NRAO.

2.2. IRAM Plateau de Bure Observations

Plateau de Bure observations were performed in the C and D configurations (the most compact ones) on September 29th 2002 and December 18th 2002 for a total of 16 hours of observing time. The correlator setup was chosen to simultaneously observe the dust continuum at 110 GHZ and 230 GHz with a 1 GHz bandwidth and the para–NH_2D(1,1) and CO(2-1) with a resolution of 0.106 km s^{-1} and 0.051 km s^{-1} respectively. Phase calibration was performed using 0528+134 and 0415+379 while absolute calibration was obtained using 3C454.3 for the D-configuration run and 3C273 for the C-configuration. The two phase calibrators have a 20% difference in flux in the two observing runs and we take this as the calibration uncertainty. Cleaning was performed with uniform weight and the resulting synthesized beam is 5.″8×4.″5 in size and 81.°4 in PA at 3 mm and 2.″5 by 2.″2 with PA 81.°0 at 1mm. The PdBI data were reduced and calibrated using the Continuum and Line Interferometer Calibration (CLIC) developed by IRAM.

3. Results

3.1. Maps and spectra

3.1.1. VLA Ammonia

In figure 1 we show the integrated intensity maps of NH_3(1,1) and (2,2) from the VLA and the 100m antenna in Effelsberg (from Tafalla et al. 2002, FWHM ≃ 37″). The qualitative difference between the two is striking: while the intensity measured with the single dish follows very closely the column density traced by the dust emission, the VLA maps of NH_3(1,1) peaks

[1] http://www.aoc.nrao.edu/∼gtaylor/csource.html

20″south-east relative to the dust peak and the NH_3(2,2) emission shows a second peak also in the north west evocative of a "hole" in the emission. The angular size of the ammonia integrated emission seen with the VLA is 75″×36″ in the (1,1) line and 68″×25″ in the (2,2) line as compared to 105″×58″ in the dust emission.

In order to properly compare the interferometer and single dish maps, we cleaned the VLA data with a 40″beam to simulate the resolution of the 100-m data. The resulting map (Fig. 1) shows that the two data sets are compatible. The discrepancy arises because the interferometer is insensitive to large scale emission and traces preferentially compact high density gas clumps. The peak intensities of these maps are a measure of the amount of flux lost in the VLA observations due to extended structure: 68% in the NH_3(1,1) (70% and 64% for the main hyperfine component and the first red hyperfine component, respectively) and more than 80% in the (2,2). As shown below the difference between these two is significant and thus the (2,2) emission appears to be more resolved out than the (1,1). This by itself is an indication that the temperature of the more extended (presumably lower density) material in the L 1544 core is higher than in the compact nucleus.

However, an important characteristic of our results is that the peak of the VLA (1,1) emission (effectively the ground state of para NH_3) is clearly not coincident with the peak of the dust emission. We believe this is mainly due to the fact that the (1,1) emission is highly optically thick and thus our measurement towards the peak of the main (1,1) satellite reflects the temperature at the surface corresponding to unity optical depth.

This is substantiated by Fig. 2 where we compare the spectra from the VLA with those observed with the single dishes. We measure at the dust peak a ratio of the satellite F=2-1 emission to the main (F=1-1 and 2-2 blend) of 0.72 as compared to the expected ratio of 0.278 in the optically thin limit. This (see e.g. Ho & Townes 1983) allows an estimate of the main line optical depth and we derive a higher value from the VLA data (with an optical depth integrated over all the hyperfine components of $\tau_{tot} > 30$) than from the 100m ($\tau_{tot} = 8.6$), while 20″ further from the peak the difference in opacity is reduced ($\tau_{tot} = 20$ vs. $\tau_{tot} = 7.7$) and a smaller amount of flux is resolved out (we recover 75% of the flux). Our optical depths are in fact so high that they may affect the temperature gradients discussed later. These issues will be treated more quantitatively in section 4.3 where we report our radiative transfer calculations combined with the u, v modelling of the emission. For the moment, we note however that these results are consistent with a high ammonia column density in the neighbourhood of the dust peak.

3.1.2. NH_2D with Plateau de Bure

Our NH_2D data are extremely useful in that they confirm that ammonia remains in the gas phase at the densities of order 10^6 cm^{-3} close to the dust peak. As in the case of ammonia, one can use the relative intensities of the hyperfine satellites to provide a measure of optical depth and in this case (see fig. 2) we find intensity ratios of the main component versus the first red component (=0.3) consistent with optically thin LTE (=0.278). Thus the fact that the NH_2D intensity (see Fig. 1) peaks at the dust peak can be considered a demonstration of the fact that NH_2D is a tracer of the dense gas in the vicinity of the dust peak. It can thus be used to measure the kinematics in this region. The angular size of the NH_2D emission seen by the interferometer is 27″×12″ as compared to the dust emission size of 105″×58″. Comparing the intensity at peak observed by the PdB with an IRAM-30m spectrum taken towards the nucleus of L 1544 we measure that 50% of the NH_2D total flux is recovered by the interferometer.

3.2. Kinematics

We used the interferometric data in order to fit the NH_3(1,1) and (2,2) and the NH_2D spectra . In this manner, we obtained maps of velocity and line-width of the various tracers. Our results here are sensitive to differential flux loss in different channels as well as to the effects of opacity but, for the reasons discussed above, these problems are unlikely to be of great importance for NH_2D. The central velocity information was used to compute the velocity gradient across the core, in analogous fashion to Caselli et al. (2002a) using N_2H^+ and N_2D^+.

The velocity maps derived in this fashion are shown in Fig. 3. NH_3(1,1) and (2,2) show the same general pattern with a total gradient of ∼9 km s^{-1} pc^{-1} with a PA of 160 degrees west of north. This pattern can be seen also in the channel maps presented in Fig 3: in both lines the emission is brighter in the north at blue velocities to become stronger in the south for higher velocities. Over a scale of 1 arc minute(0.04 parsec), this amounts to a specific angular momentum of 0.015 pc km s^{-1} or $5\,10^{21}$ cm^2s^{-1}. Our results match the velocity gradients calculated by Caselli et al. (2002a) from single–dish observations N_2D^+, showing gradients of ∼6 km s^{-1} pc^{-1} with a similar position angle as NH_3.

The different morphology of the NH_2D maps compared to those of NH_3 already tells us that the two species traces different material, this is confirmed in the velocity maps. in fact, the NH_2D velocity gradient map shows no clear sign of rotation with total gradient of ∼2 km s^{-1} pc^{-1} with a PA of 60 degrees west of north. The corresponding specific angular momentum is 0.001 pc km s^{-1} or $3.5\,10^{20}$ cm^2s^{-1}, about an order of magnitude lower than the specific angular momentum measured with NH_3. We note that the position angle obtained from NH_2D is different from that seen in N_2D^+ by Caselli et al. (2002a) and may suggest a difference between the bulk motions of neutral and ion species in the inner core.

We note that the specific angular momentum obtained from NH_3 is typical of starless cores (see e.g., Ohashi 1999), while the smaller specific angular momentum derived from NH_2D is closer to the values of protostellar envelopes. Observations with higher velocity resolution should be needed to confirm this loss of specific angular momentum towards the small scales; however, this differential rotational properties between the inner envelopes and the ambient cloud is consistent with other observations in more evolved objects (Belloche et al. 2002).

3.3. Dust Continuum and CO(2-1)

The Plateau de Bure Interferometer observations, together with the NH_2D(1,1) , simultaneously mapped L 1544 in the dust continuum at 230 GHz and 110 GHz, and in CO(2–1). These observations resulted in $3\,\sigma$ non-detections of 0.9 mJy $beam^{-1}$ and 0.5 mJy $beam^{-1}$ for the 1 mm and 3 mm continuum respectively. The corresponding limit for CO(2–1) was 80 mJy $beam^{-1}$ for the CO(2–1).

Dust and CO emission from L 1544 is easily detected by single dish telescopes (Tafalla et al. 2002), but their distribution is clearly too extended even for the most compact PdBI configurations leading to a total loss of flux. The absence of *compact* continuum emission at 1 mm confirms the starless nature of L 1544

and for an (arbitrarily) assumed temperature of 30 K yields an upper limit to the mass of a protoplanetary disk (on size scales of 1 beam i.e. 2.″5 by 2.″2) of $1.8 \cdot 10^{-4}$ solar masses. This estimate is a strong upper limit because we assume the small dust opacity for grains coated with thin ice mantles and maximum size of 0.25 μm) (equal to 0.78 cm^2 g^{-1} Ossenkopf & Henning 1994); if the maximum size of the dust grains in the disk grows to 1 mm the upper limit should be decreased by a factor of four (e.g. see dust opacities from Draine 2006). In fact, if L 1544 did contain a low-luminosity protostellar object similar to that found by the Spitzer Space Telescope in L 1014-IRS (Young et al. 2004), then we might have observed the continuum from the disk surrounding the protostar (expected to be of few mJy in L 1014-IRS at 1 mm, Young et al. 2004). We assume here low optical depth conditions appropriate for large (> 100 AU) disks observed at millimeter wavelengths. For very small optically thick disks, our result amounts to a limit of $T_{disk} < 50\,K\,(R_{disk}/1AU)^{-2}$. In any case we would have certainly observed a molecular outflow similar to that in L 1014-IRS (which was detected by Bourke et al. 2005 with a R.M.S. of 80 mJy (1″beam)$^{-1}$, i.e. 4.8 times less sensitive than the present PdBI observations).
Our data thus confirm the *starless* nature of L 1544.

4. Analysis

4.1. Evaluation of temperature in LTE

Deriving temperatures from NH_3 data has mostly been done using the so–called "standard analysis" (e.g. Ungerechts et al. 1986; Stutzki & Winnewisser 1985). One can use for example equation A7 from Ungerechts et al. (1986) to compute the "rotation temperature" T_{12} defined by the ratio of populations in then (2,2) and (1,1) levels. It is well known (Walmsley & Ungerechts 1983) that at low temperatures this is in practice close to the kinetic temperature (i.e. to LTE between the two levels). Thus,

$$T_{12} \;=\; T_{2,2}/\ln[\tau_{11}^{tot}/(0.45\,\tau_{22}^{tot})] \qquad (1)$$

where $T_{2,2}$ is the excitation energy of the (2,2) relative to the (1,1 level (41 K), and τ_{11}^{tot} and τ_{22}^{tot} are the total optical depths of the (1,1) and (2,2) levels respectively (i.e the sum over all satellites). We assume here equality of line-widths and "amplitude factors" (see Ungerechts et al. 1986)) for the two lines.

We thus see that our accuracy in determining the temperature depends on our accuracy in determining the optical depths. This is limited in the case of the (1,1) by the fact that using the relative intensities of the satellites becomes inaccurate for large optical depths (ratios close to unity). In the case of the (2,2) on the other hand, we do not measure the (2,2) satellites and thus are forced to derive the (2,2) optical depth from the ratio of the (2,2) and (1,1) main lines. Thus, we have

$$\tau_{22}^{tot} \;=\; -1/f_{22}\;\ln\left\{1-(T_{M,2}/T_{M,1})\left[1-\exp(-f_{11}\tau_{11}^{tot})\right]\right\} \qquad (2)$$

where $T_{M,2}$ and $T_{M,1}$ are the observed (2,2) and (1,1) brightness temperatures of the main hyperfine components and f_{22} and f_{11} are the relative intensities of the main hyperfine structure for the (2,2) and (1,1) (0.5 and 0.8). The error-bars were evaluated propagating the errors on $T_{M,2}$, $T_{M,1}$ and τ_{11}^{tot}. Note that doubling the intensity ratio between the (2,2) and (1,1) transitions would result in an increase of temperature of only 0.5 K, while doubling the opacity of the (1,1) transition would decrease the temperature of 0.7 K. We expect that neither the errors on the opacity determinations nor the differential flux loss between the (1,1) and (2,2) reach this. Our main errors in this approach are caused by the breakdown of the isothermal assumption and to differential flux loss between (2,2) and (1,1) (twice as much lost in (2,2)).

In panel a of Fig. 4, we present the temperatures derived using this technique as a function of projected distance from the dust peak. Both our present VLA data set and the 100-m results of Tafalla et al. (2002) are shown. For comparison, we show results from the theoretical model of Galli et al. (2002). A clear drop in temperature is found toward the continuum peak on the basis of the VLA data in contrast to the single dish data which show a rather flat profile. This is a clear suggestion that the compact high density core nucleus sampled with the interferometer is at a lower temperature than its surroundings.

Our VLA data suggest that the gas temperature in the inner nucleus reaches values as low as 6 K. This contrasts with the minimum dust temperature of 11 K derived by Ward-Thompson et al. (2002) from ISOPHOT observations between 90 and 200μm), although it should be noted that these observations were done with ∼80″ of angular resolution and that far infrared observations alone are more sensitive to extended, warmer (T > 30 K) dust coming from smaller optical depths, like the outskirts of starless cores. In fact our observations are fully consistent with the best fit of Doty et al. (2005) who modelled the dust continuum at 450, 850 and 1300 μm) (hence typical of cold dust) with a 3D radiative transfer code resulting in a central temperature of 5.4 K.

In Fig. 4 we superimposed a modified version of the theoretical prediction (green curve) made by Galli et al. (2002). Modifying the model in Galli et al. (2002) was necessary since this was calculated starting from a density profile that was derived from a constant dust-temperature of 8.75 K (Tafalla et al. 2002). Since the observed drop in gas temperature reflects a drop in dust temperature (the two are well coupled at high densities and low temperatures, see e.g. Gonçalves et al. 2004), we expect the central density to be enhanced using this new information. Since the temperature profile influences the estimate of the density profile and vice-versa, we had to iterate few times the following process; i) calculate the gas temperature from a given density profile ii) use that temperature profile to derive a new density profile fitting the 1.2 mm map iii) use this new density profile in point i). We converged after few iterations with the model represented in panel a) of Fig. 4. Note that this is **not** a fit of the temperature data but just an iterative process to make the model of Galli et al. (2002) self consistent with the 1.2 mm map. Nevertheless the agreement with the data is very good in the limits of validity of the model and the data. Including the temperature profile, the central density in L 1544 result to reach $\sim 2 \cdot 10^6$ cm^{-3} while the size of the flattened area shrinks by 30% and the slope of the density profile at large radii is not significantly changed.

4.2. Column density and Deuteration in LTE

Large deuterium enrichment is a characteristic of the high density nuclei of pre-stellar cores and it is a useful test of our understanding of the chemistry (e.g. Aikawa et al. 2005; Flower et al. 2006) to measure the [NH_2D]/[NH_3] ratio at high angular resolution. We have therefore combined our VLA and PdeB data for this purpose.

We derived the column density of NH_3 and NH_2D in the constant excitation temperature approximation (CTEX, see also Caselli et al. 2002b). In the case of NH_3, opacity and excitation temperature were derived through hyperfine structure fitting of the (1,1) transition using the formalism discussed earlier.

We assumed an ortho-to-para ratio (o/p) of 1 when doing this and used a classical partition function at the temperatures of interest to correct for the excited states. The results from single-dish data can be compared to the column densities evaluated by Tafalla et al. (2002) using the more sophisticated Monte Carlo approach. As shown in Fig 4, from the single dish data we derived a column density of NH_3 of $3.5 \cdot 10^{14}$ cm^{-2}, this, combined to a column density of H_2 of $9.4 \cdot 10^{22}$ cm^{-2} (Crapsi et al. 2005), furnishes an abundance of $3.7 \cdot 10^{-9}$ comparable to Tafalla et al. (2002). The interferometric observations give a factor of ∼2 larger column densities, which may be an under–estimate in that our (1,1) optical depths are in some positions lower limits.

In the case of NH_2D, we are not observing the ground transition ($1_{0,1} - 0_{0,0}$ at 332.8 GHz) and thus we need an estimate of the "rotation temperature". We solved this problem evaluating T_{ex} from the ground state to the observed level ($1_{1,1} - 1_{0,1}$) using Eq. 2.21 of Winnewisser et al. (1978):

$$\exp(-T_0/T_{ex}) = \exp(-T_0/T_{BB}) \times \times \frac{1 + (C_{ij}/A_{ij}) \exp(-T_0/T_k)[\exp(T_0/T_{BB}) - 1]}{1 + (C_{ij}/A_{ij})[1 - \exp(T_0/T_{BB})]}$$

where T_0 is the energy between the levels i and j, T_{BB} is the 2.7 K background, T_k the kinetic temperature, A_{ij} is the Einstein coefficient and C_{ij} is the collision rate between the levels j and i. The latter can be expressed as $C_{ij} = \sigma_{ij} \langle v_{th} \rangle n(H_2)$, where σ_{ij} is the cross section of the $i - j$ transition ($= 8 \cdot 10^{-16}$ cm^{-2}, cf. Green 1976; Turner et al. 1978), $\langle v_{th} \rangle$ is the thermal velocity dispersion and $n(H_2)$ the H_2 volume density. Taking the kinetic temperature from the NH_3 data and the $n(H_2)$ from the 1.2 mm data we were able to evaluate the excitation temperature of the ground transition and thus the partition function of NH_2D. This amounts to ignoring the splitting of the J=1 level and is a crude procedure but we think it gives a reasonable estimate of the fraction of NH_2D in the ground state. We assumed an o/p ratio of 3 for NH_2D, consistent with the average observed NH_2D o/p ratio in starless cores (Shah & Wootten 2001, but see also Flower et al. 2006 for a theoretical approach).

The column density in the level ($1_{1,1} - 1_{0,1}$) was instead calculated in the CTEX limit. The profile of $N(NH_2D)$ is shown in panel c) of Fig 4. In this case the column density derived from the interferometry data is only slightly higher than the estimate from the single dish. Dividing $N(NH_2D)$ by $N(NH_3)$ we were able to evaluate the degree of D-fractionation in NH_3at the dust peak of L 1544 (see panel d) of Fig. 4). The abundance ratio $[NH_2D]/[NH_3]$ was found to be 0.5±0.2, thus higher than in N_2H^+ (0.26, Caselli et al. 2002b), although caveats in the different flux loss between VLA and PdB apply.

4.3. Model Fits of the Temperature and NH_3 abundance

In order to account for the temperature gradient along the line of sight as well as the complex flux loss from the interferometer, we made a model of the temperature, density and abundance structure of the core. We then modelled the excitation of the molecule and the radiative transfer of the emission, and finally sampled the synthetic data cube in the u, v plane to compare with the VLA observations.

The excitation and radiative transfer calculation were performed using the 1D Monte Carlo radiative transfer code for molecular lines written by Hogerheijde & van der Tak (2000). The code takes as input for each radial cell: the density of H_2, the abundance of the molecule of interest, the dust and gas temperature and the radial velocity. Then, using the collisional rates from Danby et al. (1988) and the energy levels, transition frequencies, Einstein A coefficients (from JPL)[2] we can evaluate the population in each energy level and in each cell. This result is taken as input for the ray-tracing module to produce a data cube of the synthetic emission. We modified the ray-tracing module to include the hyperfine structure of NH_3. The output data cube can then be sampled in the u, v plane to reproduce the VLA observations. We produced such synthetic visibility datasets with the MIRIAD task UVMODEL. The Monte Carlo code used in this paper was carefully tested against the one used by Tafalla et al. (2002) resulting in a very good agreement.

We parametrized the structures of density, temperature and abundance in the following way:

$$n(r) = \frac{n_0}{1 + (r/r_{0,n})^{\alpha_n}}$$

$$X_{NH_3}(r) = X_0 (n(r)/n_0)^{\alpha_X}$$

$$T(r) = T_{out} - \frac{T_{out} - T_{in}}{1 + (r/r_{0,T})^{1.5}}$$

The forms for the density and abundance profiles where chosen for consistency with the results of Tafalla et al. (2002). The form chosen for the temperature structure has mainly the virtue of simplicity. It is consistent with those computed by Evans et al. (2001) (e.g. that shown in their Fig.6 can be represented by $T_{out} = 13.1$ K, $T_{in} = 6.5$ K and $r_{0,T} = 26''$) though we note that such models neglect the breakdown of gas-grain coupling in the outer parts of the core. We therefore ran the calculation for a grid of values for T_{out}, T_{in}, $r_{0,T}$, X_0, α_X and compared the results with the observations of the NH_3(1,1) main and first hyperfine components and the NH_3(2,2) main component observed at VLA and Effelsberg. The density distribution is not constrained by the NH_3 observations but by the 1.3 mm dust continuum. For each temperature distribution we then recomputed the density distribution that would fit the 1.3 mm observations in similar fashion to Tafalla et al. (2002).

The quantities we wish to match with both the VLA and the Effelberg observations are

- the integrated amplitude vs. u, v distance profile for each of the components (NH_3(1,1) main and first hyperfine (hf) and NH_3(2,2) main)
- the profile of the ratio between $NH_3(2,2)$/ $NH_3(1,1)_{hf}$ (which roughly speaking is a measure of the temperature) and the ratio between $NH_3(1,1)_{main}$/ $NH_3(1,1)_{hf}$ (which roughly speaking is a measure of the column density)
- the line profile of all the observed data

We compared the amplitude profile both versus the u, v distance of the baselines and versus the distance to the centre of the source in the inverted image[3]. Those plots are equivalent since they differ only for a Fourier transform, however since the plot of amplitude versus distance from the source centre shows better the emission in the centre of the source we choose to present only those plots.

The model that was found to best fit all this quantities has $T_{out} = 12$ K, $T_{in} = 5.5$ K, $r_{0,T} = 18''$, $X_0 = 8 \cdot 10^{-9}$, $\alpha_X = 0.16$.

[2] these informations are collected in the Leiden Atomic and Molecular Database at http://www.strw.leidenuniv.nl/~moldata/

[3] for this comparison we did not "clean" either the data or the model since this would have introduced further uncertainties; comparing the "dirty" maps is instead exactly equivalent to the comparison in the u, v–amplitude plane.

The density, temperature and abundance profiles of this model are shown in fig. 5 in solid lines. As a comparison we show with dashed lines the profiles relative to the best fit of the single–dish data alone with constant temperature (Tafalla et al. 2002). The new temperature profile is warmer in the outside and colder in the very centre and this results in a more peaked density structure ($n_0 = 2.1\,10^6$ cm^{-3}, $r_{0,n} = 14''$, $\alpha_n = 2.5$). The abundance rise in the centre of the core shown by Tafalla et al. (2002) is required also in our best fit although it is less steep ($\alpha_X = 0.16$ vs 0.3).

The reason for these changes in the temperature structure can be seen in the comparison between the observations and the predictions of the two models presented in Fig 6. In each panel of Fig 6 the data are shown in grey, the black–bold curves represent the prediction of our best fit model while the thin–red lines show the best fit of the single dish data assuming constant temperature. The lower temperature in the centre is required to fit the intensity of the NH_3(2,2) line which is highly over produced in the constant temperature model (see panels g and l). Lowering the central temperature requires the external temperature to be increased in order to still fit the single dish observations of NH_3(2,2) (panel c). The quality of this new temperature profile can be checked also against the ratio of the NH_3(2,2) and the $NH_3(1,1)_{hf}$ which is very sensitive to variations in the temperature profile (panel h). The constant temperature predictions are dramatically different from the observed ratio of $NH_3(2,2)/NH_3(1,1)_{hf}$. Adjustments to the abundance profile are finally needed to fit the intensity profile of the two observed NH_3(1,1) hyperfine components. The characteristic profile of the $NH_3(1,1)_{main}$ (panel e) and the flux loss of the central channels of the main component (panel k) are two sensitive indicators of a good fit to the abundance profile. In panel d the ratio between the two NH_3(1,1) hyperfine components shows the overall quality of the adopted abundance profile. We note that the best fit of Tafalla et al. (2002) better reproduces the intensity profile of the first red hyperfine component of NH_3(1,1) observed with the single–dish (panel b and i). However increasing the intensity of the $NH_3(1,1)_{hf}$ would require higher abundances or warmer inner temperatures and this would significantly worsen the modelling of the interferometric data (see panels d, f and h). A possible solution of the problem could be found introducing a 2D geometry (see e.g. the rotationally flattened envelopes of Ulrich 1976) but, since the effect on the temperature profile would be modest, this is beyond the scope of the present paper.

5. Conclusions

We presented high-resolution, interferometric observations of NH_3 and NH_2D toward L 1544, a low-mass starless core on the verge of forming a star. The gas temperature and deuterium fractionation are derived for the first time with a resolution smaller than 800 AU. The main results of this work are:

1) The gas temperature drops to ∼5.5 K at the core density peak, in agreement with theoretical model predictions (Zucconi et al. 2001; Evans et al. 2001; Galli et al. 2002) and with the continuum modelling of Doty et al. (2005). In particular, our data can be reproduced by the models of Galli et al. (2002), simultaneously fitting the dust continuum data. A similar conclusion about the gas temperature drop has been obtained by Pagani et al. (2007) based on N_2H^+, N_2D^+, and NH_3 observations of L 183.

2) The central density derived from literature data but including the temperature profile reaches $2 \cdot 10^6$ cm^{-3}, 50% higher than considering constant temperature at 8.75 K.

3) The column densities for both NH_3 and NH_2D are (factor of ∼2) larger than previously found with single-dish antennas (Tafalla et al. 2002; Shah & Wootten 2001), evidence that we are probing a higher density gas and that, unlike CO, the ammonia freeze–out is not significant in the core centre, where $n(H_2) \gtrsim 10^6$ cm^{-3}.

4) The deuterium fractionation in NH_3 is 0.5±0.2, almost constant in the central 4000 AU, where NH_2D is detected

5) The NH_2D map, unlike those of NH_3, peaks at the dust continuum peak showing that it is a very good tracer of the high density gas. A comparison between the velocity field extracted from NH_2D with the one derived from NH_3 shows an order of magnitude decrease of specific angular momentum from the large scales to the small scales.

Acknowledgements. We gratefully thank the IRAM-Plateau de Bure staff and NRAO-VLA staff, and in particular Clemens Thum, Roberto Neri and Yancy Shirley, for support in preparing and performing these observations A special thanks goes to Dr. Riccardo Cesaroni and Dr. Michiel Hogerijde for extensive help in the data reduction and analysis and to Jose Gonçalves for running a modified version of his temperature model. A.C. acknowledges dr. Marcello Giroletti and dr. Lara Baldacci for interesting discussions that improved this manuscript. A.C. was supported by a fellowship from the European Research Training Network "The Origin of Planetary Systems" (PLANETS, contract number HPRN-CT-2002-00308) at Leiden Observatory.

References

Aikawa, Y., Herbst, E., Roberts, H., & Caselli, P. 2005, ApJ, 620, 330
Bacmann, A., André, P., Puget, J.-L., Abergel, A., Bontemps, S., & Ward-Thompson, D. 2000, A&A, 361, 555
Belloche, A., André, P., Despois, D., & Blinder, S. 2002, A&A, 393, 927
Bergin, E. A., Maret, S., van der Tak, F.F.S., Alves, J., Carmody, S., Lada, C.J. 2006 ApJ, 645, 369
Bourke, T. L., Crapsi, A., Myers, P. C., Evans, N. J., Wilner, D. J., Huard, T. L., Jørgensen, J. K., & Young, C. H. 2005, ApJ, 633, L129
Caselli, P., Walmsley, C. M., Zucconi, A., Tafalla, M., Dore, L., & Myers, P. C. 2002a, ApJ, 565, 331
Caselli, P., Walmsley, C. M., Zucconi, A., Tafalla, M., Dore, L., & Myers, P. C. 2002b, ApJ, 565, 344
Crapsi, A., Caselli, P., Walmsley, C. M., Myers, P. C., Tafalla, M., Lee, C. W., Bourke, T. L. 2005, ApJ, 619, 379
Danby, G., Flower, D. R., Valiron, P., Schilke, P., & Walmsley, C. M. 1988, MNRAS, 235, 229
Doty, S. D., Everett, S. E., Shirley, Y. L., Evans, N. J., & Palotti, M. L. 2005, MNRAS, 359, 228
Draine, B. T. 2006, ApJ, 636, 1114
Evans, N. J., Rawlings, J. M. C., Shirley, Y. L., & Mundy, L. G. 2001, ApJ, 557, 193
Flower, D. R., Pineau Des Forêts, G., & Walmsley, C. M. 2006, A&A, 449, 621
Galli, D., Walmsley, M., & Gonçalves, J. 2002, A&A, 394, 275
Gonçalves, J., Galli, D., Walmsley, M. 2004, A&A, 415,617
Green, S. 1976, J. Chem. Phys., 64, 3463
Ho, P. T. P., & Townes, C. H. 1983, ARA&A, 21, 239
Hogerheijde, M. R., & van der Tak, F. F. S. 2000, A&A, 362, 697
Kirk, J. M., Ward-Thompson, D., & André, P. 2005, MNRAS, 360, 1506
Leung, C. M. 1975, ApJ, 199, 340
Lesaffre, P., Belloche, A., Chièze, J.-P., & André, P. 2005, A&A, 443, 961
Ohashi, N. 1999, Star Formation 1999, Proceedings of Star Formation 1999, held in Nagoya, Japan, June 21 - 25, 1999, Editor: T. Nakamoto, Nobeyama Radio Observatory, p. 129-135, 129
Ossenkopf, V., & Henning, T. 1994, A&A, 291, 943
Pagani, L., et al. 2004, A&A, 417, 605
Pagani, L., Bacmann, A., Cabrit, S., & Vastel, C. 2007, ArXiv Astrophysics e-prints, arXiv:astro-ph/0701823
Shah, R. Y., & Wootten, A. 2001, ApJ, 554, 933
Stutzki, J., & Winnewisser, G. 1985, A&A, 148, 254
Tafalla, M., Myers, P. C., Caselli, P., Walmsley, C. M., & Comito, C. 2002, ApJ, 569, 815
Tafalla, M., Myers, P. C., Caselli, P., & Walmsley, C. M. 2004, A&A, 416, 191
Turner, B. E., Zuckerman, B., Morris, M., & Palmer, P. 1978, ApJ, 219, L43
Ungerechts, H., Winnewisser, G., Walmsley, C. M. 1986, A&A, 157, 207
Ulrich, R. K. 1976, ApJ, 210, 377
Walmsley, C. M., Ungerechts, H. 1983, A&A, 122, 164
Ward-Thompson, D., Motte, F., & Andre, P. 1999, MNRAS, 305, 143

Ward-Thompson, D., André, P., & Kirk, J. M. 2002, MNRAS, 329, 257
Winnewisser, G., Churchwell, E., and Walmsley, C.M. 1978, in Modern Aspects of Microwave Spectroscopy, ed. Academic Press, New York, 336
Young, C. H. et al. 2004, ApJS, 154, 396
Zucconi, A., Walmsley, C. M., & Galli, D. 2001, A&A, 376, 650

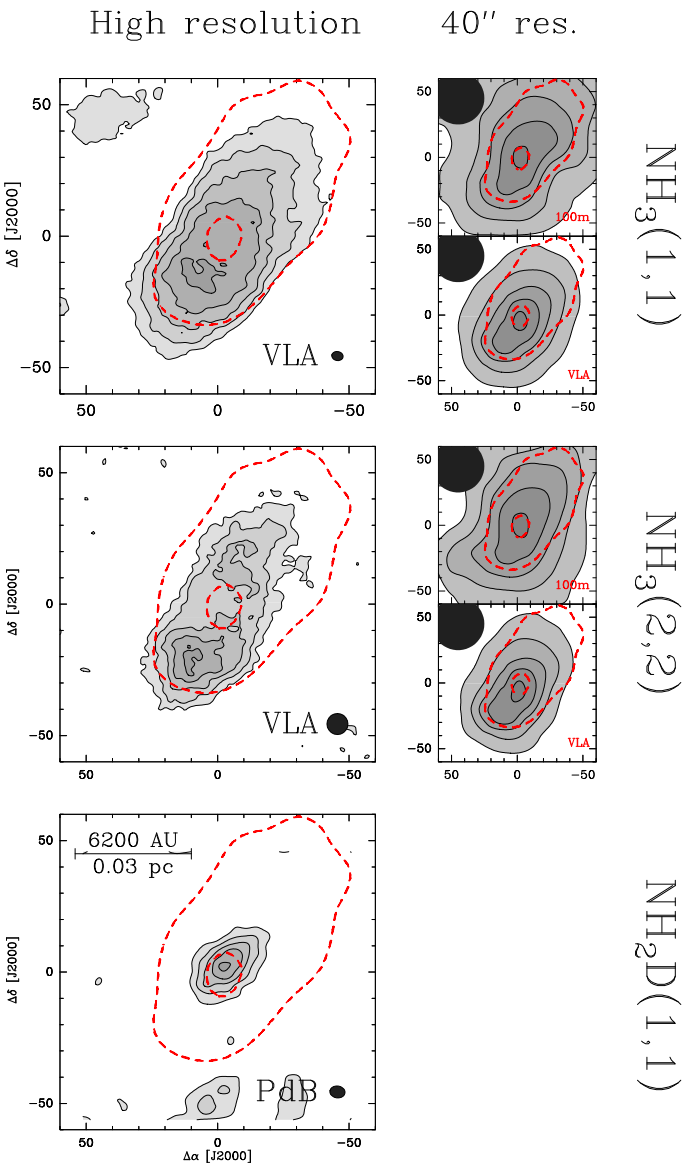

Fig. 1. Integrated intensity maps of L 1544 in NH_3(1,1) and (2,2) and para–$NH_2D(1_{11} - 1_{01})$. Dashed contours in all the panels are the 50% and 95% levels of the 1.2mm continuum taken from Ward-Thompson et al. (1999) and smoothed to 22″. **Left column:** Observations taken with VLA or PdBI were integrated over all the hyperfines available (NH_3(1,1) values refer only to the main component and the first red component). Angular resolution is 4.″34×3.″45, 8″and 5.″8×4.″5 for NH_3(1,1), NH_3(2,2) and NH_2D(1-1), respectively, and it is reported in the bottom right. Levels are 15% to 95% by 20% of the map peak which is 0.25, 0.05 and 7.0 K km s^{-1} for NH_3(1,1), NH_3(2,2) and NH_2D(1-1), respectively. **Right column:** Integrated intensity maps of the observations from the single dish (top) and interferometer data smoothed to 40″(bottom). Levels are spaced percentually as in the left column but peak values are 8.5 K km s^{-1}and 2.8 K km s^{-1}for the single dish map of NH_3(1,1), and the smoothed VLA map of NH_3(1,1), and 0.47 K km s^{-1}and 0.08 K km s^{-1}for the NH_3(2,2) maps from Effelsberg and VLA. A 40″ beam is reported at the top-left corner.

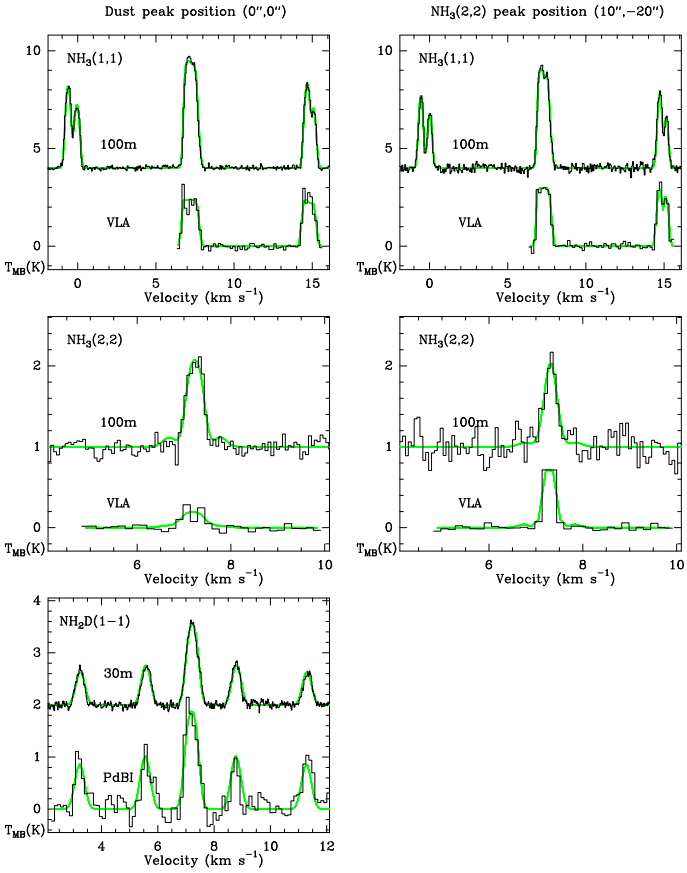

Fig. 2. Comparison between NH_3(1,1) and (2,2) and NH_2D(1-1) spectra observed with the interferometers (VLA and PdBI) and the same line observed with the single-dish (100m in Effelsberg and IRAM-30m). The three left box show the spectra observed toward the dust emission peak while the two right ones were taken toward the NH_3(2,2) peak (offset by 10″,-20″).

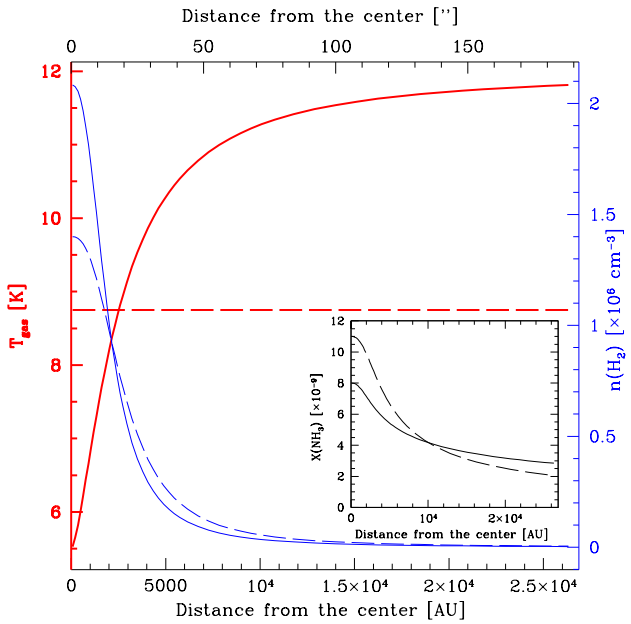

Fig. 5. Temperature, density and NH_3 abundance profile that best fit the interferometric and the single dish observations simultaneously (solid lines). The profiles relative to the best fit to the single dish data alone by Tafalla et al. (2002) are reported in dashed lines for comparison.

List of Objects

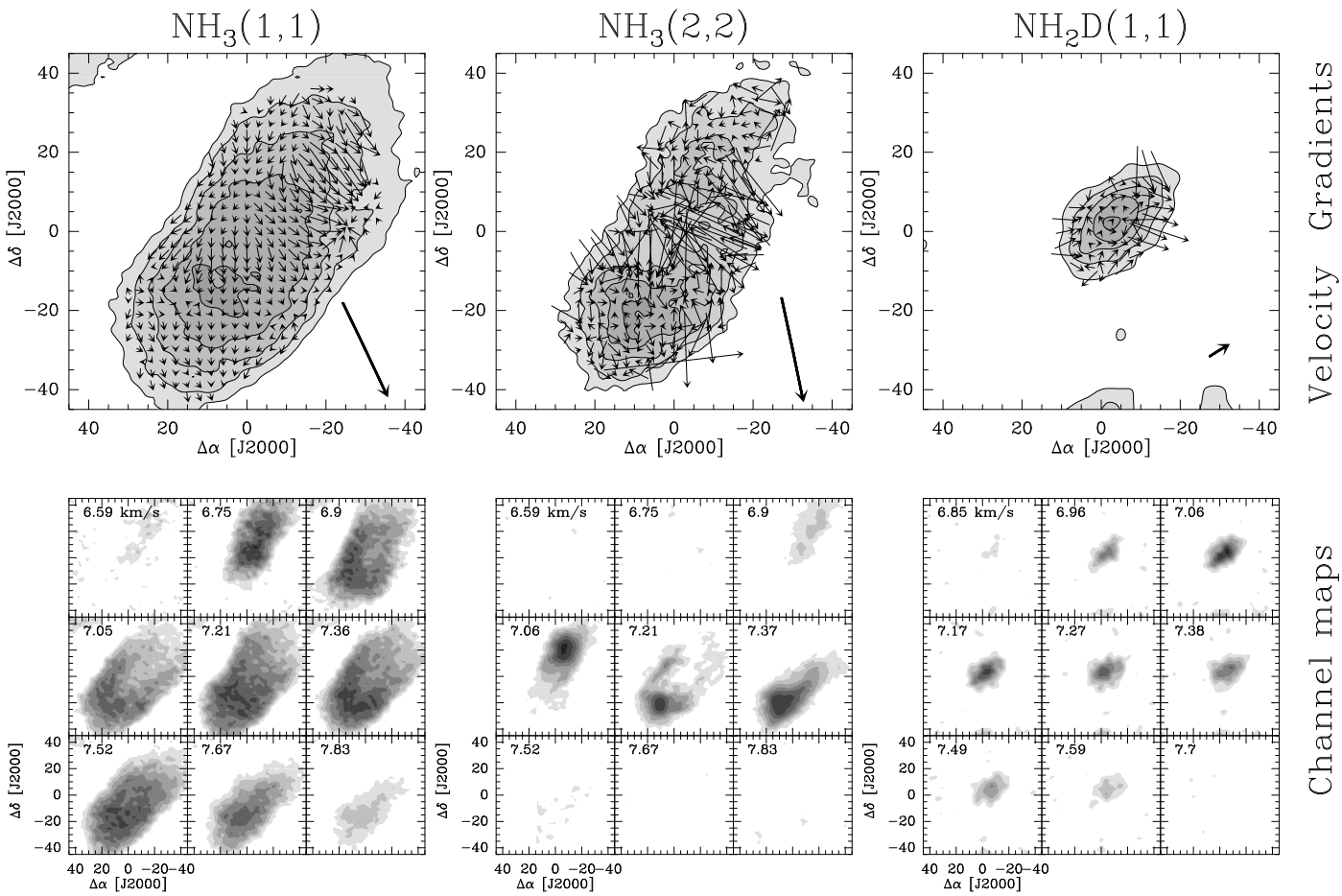

Fig. 3. Kinematics in L 1544. **Top row:** velocity gradients calculated in 9 adjacent points are overlaid on the integrated intensity map for each observed transition. The direction of the arrow points to the increasing velocity while the lenght measure the magnitude of the gradient (a 10″ arrow corresponds to a gradient of 33 km s^{-1} pc^{-1}). The thick arrows in the bottom-right represent the total gradient evaluated with all the fits (the magnitude for those is ten times smaller: i.e. a 10″ arrow corresponds to a gradient of 3.3 km s^{-1} pc^{-1}) **Bottom row:** channel maps of the main component of each observed line (VLA and PdBI).

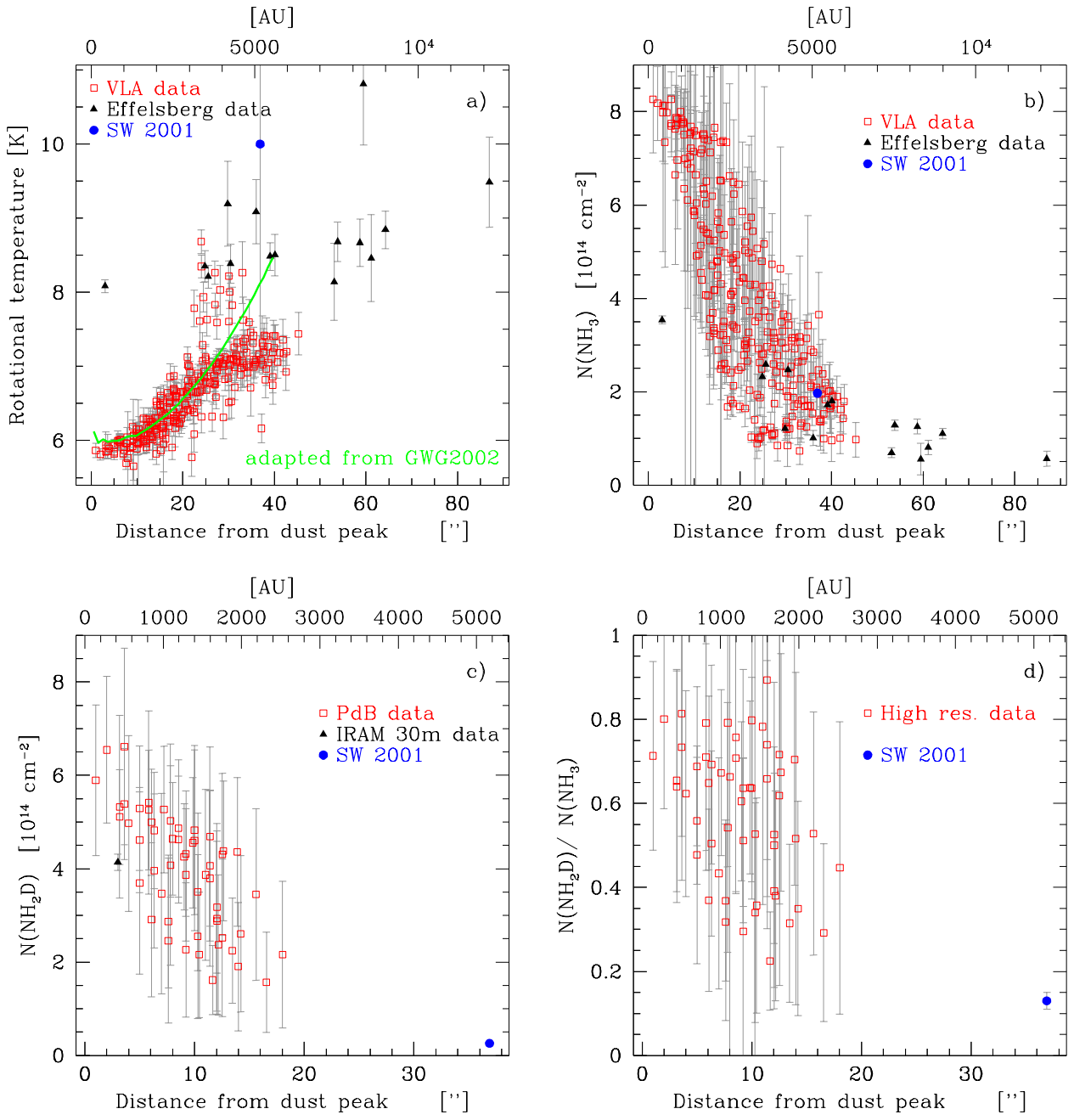

Fig. 4. Temperature and column densities profiles as derived in the LTE approximation (see sections 4.1 and 4.2). Observations from VLA are represented with empty squares, while those obtained at the 100m single-dish in Effelsberg are shown with filled triangles. Literature data from Shah & Wootten (2001) are shown with filled circles. **Panel a):** Gas temperature profile in L 1544 both from single-dish (triangles and circle) and VLA data (empty squares). The solid line is an adaptation of the Galli et al. (2002) model now using a central density of $2 \cdot 10^6$ cm^{-3} which is consistent with the low temperature observed (see section 4.1). **Panel b):** NH_3 column density profile from both single dish data (triangles and circle) and VLA data (empty squares). **Panel c):** same as panel b) but for NH_2D. **Panel d):** $N[NH_2D]/N[NH_3]$ profile for the literature data and the new high-resolution data.

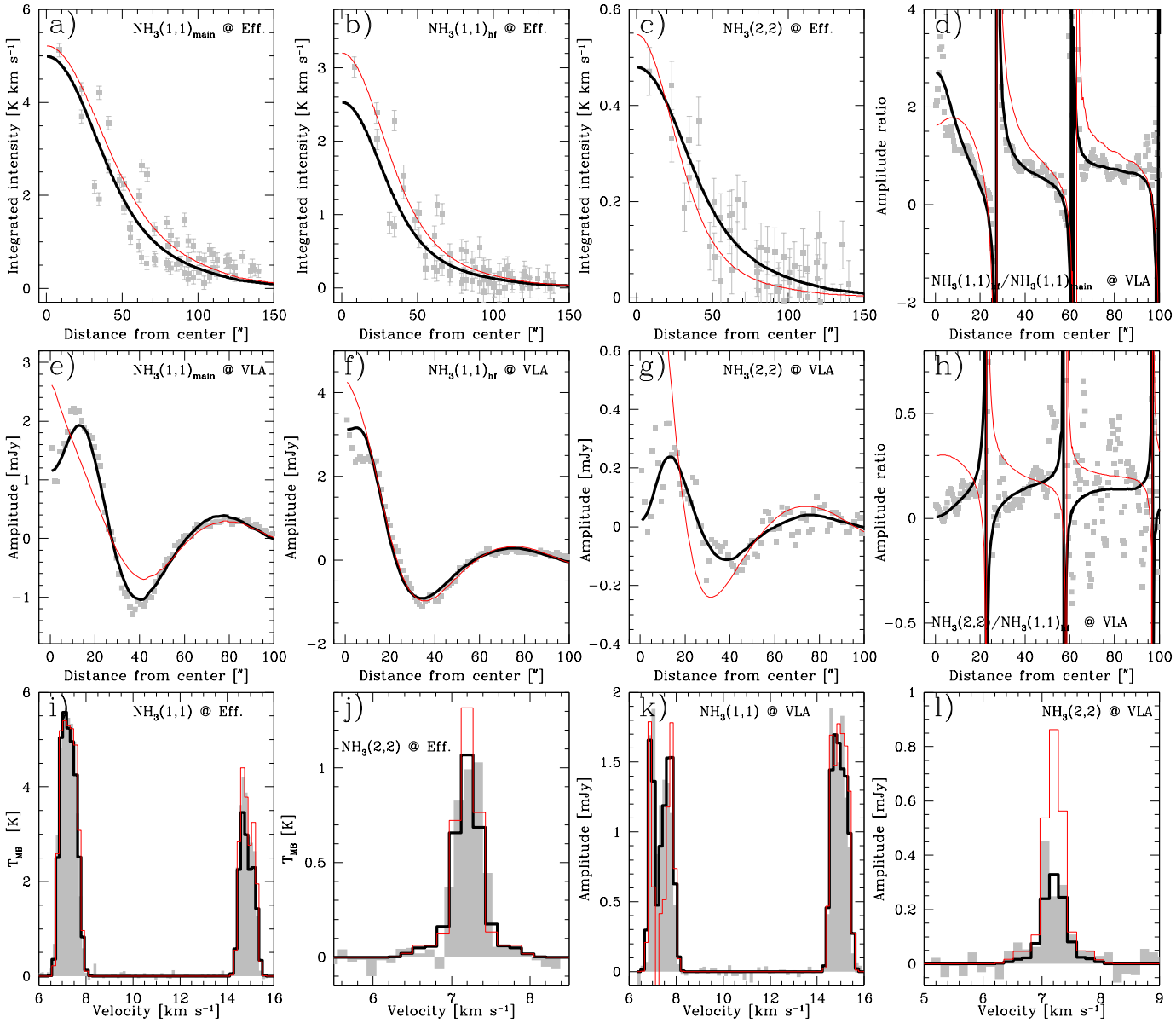

Fig. 6. Comparison between the observations of NH_3(1,1) and (2,2) taken with the 100m antenna of Effelsberg and the VLA, and the model prediction. Data are always displayed in light grey. The best fit is shown in bold black lines, while the thin red curves show the best fit of the single dish data alone. In panel a) we show the integrated intensity of the main hyperfine component of NH_3(1,1) as observed with the single-dish. Panel b) and c) are similar to panel a) but for the first red hyperfine component of NH_3(1,1) and the main component of the NH_3(2,2). Panels d) to h) present the intensity profiles observed with the VLA compared with the models. Both the data and the models were inverted from the *u*, *v* plane to the image plane using a fast fourier transform and then azimuthally averaged; the consequent negative values are not due to errors but to the negative side-lobes, and we chose to include them in the modelling rather than add further uncertainties due to cleaning. In panel d), we show the intensity ratio profile between the first red hyperfine component of NH_3(1,1) and the main component, this is an indicator of column density distribution; the asymptotic behaviour at 25″ and 60″ is due to the different extension of the two maps that determine a different size of the negative side-lobes. In panel e), f) and g) we present the intensity profiles of the NH_3(1,1) main component, NH_3(1,1) first red hyperfine and NH_3(2,2) main component, respectively. Panel h) shows the amplitude ratio profile between the NH_3(2,2) main component and the first red hyperfine component of NH_3(1,1), this is an indicator of temperature. From panels i) to l) we compare the spectra at peak observed with the single dish and the interferometer with the models.